Discrete, Dispersible MnAs Nanocrystals from Solution Methods: Phase Control on the Nanoscale and Magnetic Consequences

Keerthi Senevirathne,[†] Ronald Tackett,[‡] Parashu Ram Kharel,[‡] Gavin Lawes,[‡] Kanchana Somaskandan,[†] and Stephanie L. Brock[†,*]

[†]Department of Chemistry, Wayne State University, Detroit, Michigan 48202, and [‡]Department of Physics and Astronomy, Wayne State University, Detroit, Michigan 48201

ABSTRACT Nanocrystals of thermodynamically stable α-MnAs (hexagonal NiAs-type) and metastable β-MnAs (orthorhombic MnP-type) have been synthesized by the reaction of triphenylarsine oxide (Ph_3AsO) and dimanganesedecacarbonyl (Mn_2CO_{10}) at temperatures ranging from 250 to 330 °C in the presence of the coordinating solvent trioctylphosphine oxide (TOPO). Morphologically, both α- and β-MnAs nanoparticles adopt a core—shell type structure with a crystalline core and low-contrast noncrystalline shell. In contrast to prior studies on MnAs particles, disks, and films, the present bottom-up synthesis yields discrete, dispersible MnAs nanoparticles without a structural support. Even in the absence of epitaxial strain, the lattice parameters of the nanocrystals are decreased relative to bulk MnAs, resulting in a volume decrease of 0.35% in α-MnAs and 0.38% in β-MnAs nanoparticles. In contrast to bulk MnAs, where the ferromagnetic phase transition upon warming through 313—317 K is concomitant with a structure change from ferromagnetic α- to paramagnetic β-MnAs, powder X-ray diffraction studies suggest there is no conversion of α-MnAs to β over the temperature range 298—343 K. Moreover, magnetic measurements suggest that both α- and β-MnAs are ferromagnetic with $T_C \approx 315$ K. Partial phase transformation of β-MnAs nanoparticles into thermodynamically stable α-MnAs occurs slowly over time (*i.e.*, months) at room temperature. However, there is no associated change in magnetization, suggesting the ferromagnetism observed in β-MnAs is intrinsic and cannot be attributed to α-MnAs impurities.

KEYWORDS: manganese arsenide · nanoparticles · synthesis · magnetism · phase change

Over the past decade, MnAs has become a focus of intense research due to the interesting magnetic and structural properties it exhibits and its potential to address key technological issues in information storage/processing and energy applications. Bulk MnAs shows a transition from ferromagnetic order to paramagnetism on warming through 313−317 K, concomitant with a first-order structural transition from the hexagonal α-MnAs (NiAs-type) structure to the orthorhombic β-MnAs (MnP-type) structure (Figure 1).[1] A second-order phase transition from the β structure to the α structure is complete by $T = 398$ K, the extrapolated T_C for α-MnAs.[2] The first-order phase transition temperature is a sensitive function of Mn−Mn and Mn−As distances in the material and can thus be tuned by external physical pressure[2,3] or internal chemical pressure, the latter achieved by P-doping.[4] The coupling between the magnetic transition and structural transition is sufficiently robust that the structural transition can be driven by application of a magnetic field.[5]

Materials that show magnetostructural phase transformations have technological applications in magnetic refrigeration[6] owing to their large magnetocaloric effects, which are magnified near the transition.[7] They are also of interest for thermally assisted magnetic recording devices in that information can be erased by heating through the transition.[8] Additionally, epitaxially grown MnAs is an attractive candidate as the ferromagnetic component for spin injection into III−V based semiconductors such as GaAs or InP (despite the sizable lattice mismatch) because high quality interfaces can be achieved.[9]

Most reports on nanoscale MnAs have focused on the synthesis of films or disks, with few studies on the preparation of nanoparticles. In all cases, these syntheses are limited to nanoscale MnAs prepared by epitaxial growth on (or within) III−V semiconductors, or Si. Among the characteristics observed experimentally, the magnetic relaxation occurs very slowly at 300 K because the uniaxial magnetocrystalline anisotropy is large and stabilizes the magnetization,[8] and it is possible to induce single particle (nanobit) switching using a relatively small magnetic field (60 Oe).[10] Of particular relevance to the present study is the

*Address correspondence to sbrock@chem.wayne.edu.

Received for review February 25, 2009 and accepted April 02, 2009.

Published online April 9, 2009.
10.1021/nn900194f CCC: $40.75

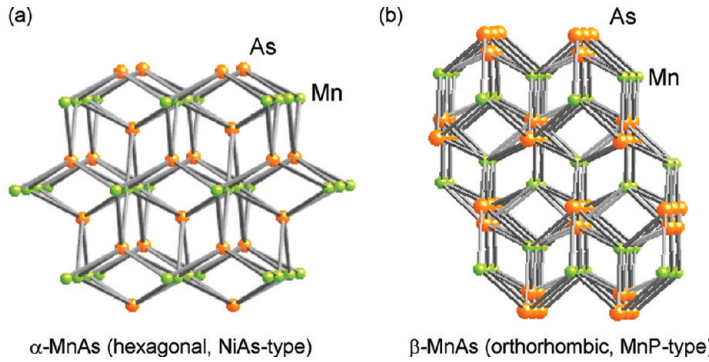

Figure 1. Illustration of the two polymorphs of MnAs (a) α-MnAs (view down c_{hex} axis) and (b) β-MnAs (view down a_{ortho} axis; $a_{ortho} = c_{hex}$).

coexistence of α- and β-MnAs in 250 nm thick MnAs films in a temperature range of approximately 300−316 K[11] and also observed in 75−800 nm diameter disks[8] at 302 K, both grown on GaAs. The coexistence arises due to discontinuous strain, and the temperature range over which this occurs may change based on the dominant strain (tensile or compressive, imposed by thermal expansion mismatch of MnAs and substrate or volume change of MnAs, respectively).[12] Because previously studied MnAs nanoparticles have been prepared epitaxially and are therefore strained, the intrinsic properties of MnAs particles remain unknown.

In contrast to top-down and vapor-phase deposition methods used previously, bottom-up arrested precipitation allows for the formation of support-free nanoparticles, thereby enabling the intrinsic size-dependent properties to be probed. Such methods have been extensively used for the preparation of a wide range of metal oxides, chalcogenides, phosphides and, to a lesser extent, arsenides.[13−22] However, there are no reports of MnAs nanoparticles prepared by this approach. In this paper, we establish that we can prepare either the room-temperature thermodynamically stable α-phase or metastable β-phase as single-phase discrete nanoparticles with narrow polydispersity by careful control of synthesis parameters. The temperature-dependent magnetic and structural characteristics are evaluated and the consequences of spatial isolation of the nanoclusters for the magnetostructural transition discussed.

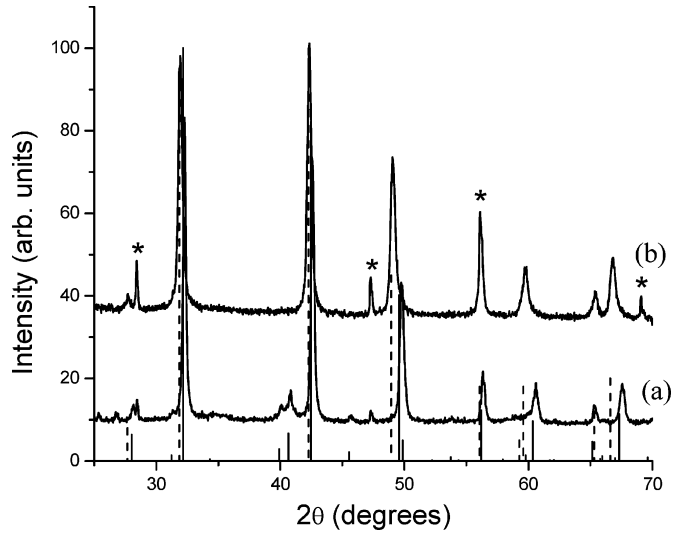

Figure 2. PXRD patterns of particles prepared by (a) high temperature synthesis (β-MnAs) and (b) slow heating (α-MnAs). The line diagrams are the reference patterns for α-MnAs (dashed lines, PDF no. 28-0644) and β-MnAs (solid lines, PDF no. 71-0923). Peaks arising from the Si standard are marked with stars.

RESULTS AND DISCUSSION

Synthesis. Two different temperature protocols were employed for the synthesis of discrete nanoparticles of MnAs: (1) rapid injection of reagents at high temperature (330 °C) and (2) slow heating to a moderate temperature (250 °C).

MnAs Nanoparticles from High Temperature Synthesis (330 °C). Dimanganese decacarbonyl [$Mn_2(CO)_{10}$] and triphenylarsine oxide (Ph_3AsO), were dissolved in octadecene (OD) and rapidly injected into trioctylphosphine oxide (TOPO) maintained at 330 °C. The colorless TOPO solution turns black within minutes, suggesting rapid nucleation of nanoparticles. After 18 h of reaction time, nanoparticles were isolated by precipitation using chloroform as the solvent and methanol as the antisolvent, followed by centrifugation. This process was followed by several washing and precipitation cycles.

Powder X-ray diffraction (PXRD) analysis was used to collect structural and crystallite size information (Figure 2a). The nanoparticles were crystalline, as evidenced by sharp diffraction peaks, and can be indexed to β-MnAs (orthorhombic MnP-type). This is a surprising result, because the β-phase is not expected to be stable at room temperature. The observed pattern, while matching well in terms of number of peaks and relative intensities, is shifted to higher 2θ relative to the reference pattern for β-MnAs. Least-squares refinement of the PXRD pattern suggests the lattice parameters along the *b* and *c* axes are reduced relative to the reference parameters for β-MnAs (Table 1). As a result, the unit cell volume of β-MnAs is decreased by 0.38%. While significant, the change in lattice parameters is not sufficient to explain the observed stabilization of the β-phase at room temperature. The unique compression of the bc axis is expected to lead to a decrease in the phase change temperature, but based on the model proposed by Iikawa and co-workers,[23] this should only be ~10 K, suggesting that the α-phase should be stable up to ca. 303−307 K and that we should be observing the α-phase at room temperature, in contrast to our observation.

To prove that the room-temperature stability of β-MnAs and the lattice contraction are not due to adventitious P-doping from the reaction with TOPO, the elemental composition of β-MnAs, both as-prepared and $CHCl_3$-washed, was determined by energy dispersive spectroscopy (EDS). The as-prepared sample had a composition of 41.9 atom % Mn, 40.4 atom % As, and

TABLE 1. Crystallite and Particle Sizes, Lattice Parameters, and Unit Cell Volumes of MnAs Nanoparticles, Along with Lattice Parameters of Bulk MnAs; Percentage Difference from Bulk Lattice Parameters and Volume Are Also Shown

		particle size (nm)[b]		lattice parameters (Å)			
MnAs phase	crystallite size (nm)[a]	core	core+shell	a	b	c	volume (Å^3)
β-MnAs	26.0 ±0.8	28.1 ±3.1	35.1 ±1.9	5.7236 (21)	3.6689 (15)	6.3484(29)	133.31
				+0.00%[d]	−0.09%	−0.29%	−0.38%
β-MnAs[c]				5.7200	3.6760	6.3790	133.82
α-MnAs	25.0 ±0.5	25.3 ±1.6	29.6 ±0.9	3.7088 (27)	3.7088 (27)	5.7022 (4)	68.19
				−0.30%[d]	−0.30%	−0.14%	−0.35%
α-MnAs[c]				3.7220	3.7220	5.7020	68.43

[a]Based on PXRD data. [b]Based on TEM data. [c]Based on reference 24. [d]Percentage lattice parameter or volume difference from bulk.

17.7 atom % P. Washing the samples with $CHCl_3$ yields a material with a nearly 1:1 Mn:As atom ratio (50.6:49.4), but no detectible P (Figure S1, Supporting Information). This suggests the phosphorus in as-prepared samples comes uniquely from TOPO surface capping groups and that the formation of β-MnAs and lattice parameter contraction is not a consequence of unintentional P-doping. We are not able to rule out the possibility that the contraction arises from light element doping because the instrument used for EDS does not detect elements with $Z \leq 11$. Alternatively, it is possible that the contracted lattice parameters arise from the amorphous shell inducing compressive strain within the core.

The morphology and size distribution of β-MnAs nanoparticles were investigated using transmission electron microscopy (TEM). A representative TEM image of β-MnAs is shown in Figure 3a along with a high resolution (HR) image (inset) and size distribution histogram. The TEM micrograph indicates that β-MnAs nanoparticles exhibit a nearly spherical shape with a high degree of crystallinity, as evidenced by the presence of lattice fringes in the HRTEM image. However, these particles have a low contrast shell that appears to be amorphous. The average crystallite core size of β-MnAs is ~28 nm with core sizes ranging from 14−46 nm. The statistical core particle size calculated from TEM micrographs agrees well with the crystallite sizes calculated by the application of the Scherrer formula[25] to powder X-ray diffraction patterns, 26 nm, based on the full width at half-maximum (fwhm) of the peak at $2\theta = 32.16°$ [(111) reflection]. This is consistent with the expectation that the low contrast "shell" is due to an amorphous coating.

Moderate Temperature Synthesis of MnAs Nanoparticles (250 °C). During the studies described above, we found that some of the nanoparticle syntheses yielded X-ray diffraction patterns suggestive of a mixture of α and β-phases, thus suggesting that α-phase MnAs nanoparticles may also be accessible under suitable reaction conditions. After evaluating a range of synthetic conditions, we determined that the α-phase is best prepared by slow heating (in lieu of rapid injection) at moderate temperatures. The synthesis was performed by heating all the molecular components in one flask slowly up to 200 °C over a period of ca. 2 h and then directly increasing the temperature to 250 °C. It was possible to follow the reaction progress by the color changes visible at different temperatures. The initial yellow solution passes through pale brown, reddish brown, and finally becomes black. Particle isolation is similar to that carried out for β-MnAs. Interestingly, injection of the precursor mixture of $Mn_2(CO)_{10}$ and Ph_3AsO in octadecene into hot TOPO (T = 250 °C) does not yield an isolable product.

The PXRD pattern for the MnAs nanoparticles synthesized at 250 °C shows that the nanoparticles adopt the α-MnAs (hexagonal NiAs-type) structure (Figure 2b). Both *a* and *c* lattice parameters are compressed, with the *a*-axis lattice parameter for the nanoparticles showing a larger reduction relative to bulk α MnAs than the *c*-axis parameter, leading to a decrease in unit cell volume of 0.35% (Table 1), similar to that noted for β-MnAs. The calculated crystallite size is also similar to that obtained for β-MnAs ~25.0 nm (Table 1) and these nanoparticles also show a core−shell type structure suggestive of a crystalline core and amorphous shell. The average core particle size computed for α-MnAs by TEM (using the smallest dimension of the ellipse) is approximately 25 nm, which correlates well with the size obtained from PXRD data. Despite many similarities, the α-MnAs nanoparticles can be readily differentiated from β-MnAs because the former adopt a characteristic elliptical shape (Figure 3b).

Structural Phase Transitions. We conducted temperature dependent PXRD measurements to carefully probe the possibility of a structural phase transition in these nanoparticle samples. On the basis of the behavior of bulk MnAs, as well as reports for epitaxially prepared MnAs nanoparticles, we anticipated that the transition from α to β would occur in the vicinity of 315 K. Figure 4 shows X-ray diffraction patterns acquired *in situ* for an α-MnAs nanoparticle sample over a temperature range from room temperature to 343 K and a 2θ range of 35−45°. This is the range where the two small, but characteristic, peaks of β-MnAs would be expected to appear during the first-order transition from α to β, the appearance of which could be unequivocally attributed

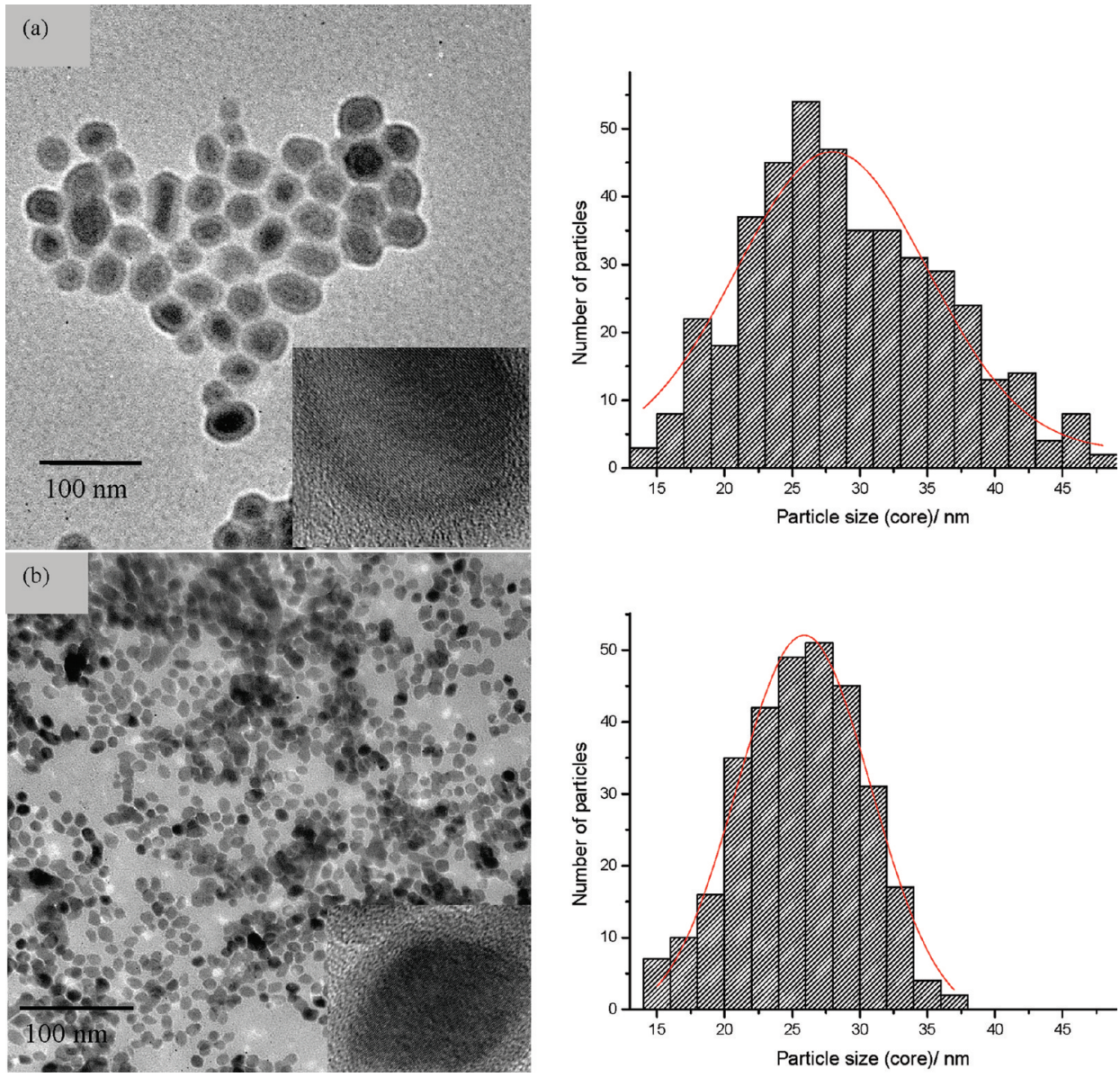

Figure 3. TEM micrographs and core size distribution histograms (a) of β-MnAs nanoparticles and (b) α-MnAs nanoparticles. The insets show HRTEM micrographs of a single crystalline particle and the amorphous shell.

to a phase change. While the peak from the Pt heater would obscure the peak at 39.8°, the peak at 40.7° should be resolvable and the intensity (relative to the peak at 42.5°) detectable if present. However, we observe no change in the peak pattern upon heating through this temperature range, suggesting that the characteristic structural transformation of the bulk phase is absent in the nanoparticles, or increased to much higher temperatures than in bulk MnAs.

Other measurements also suggest that structures can be kinetically trapped in the discrete MnAs nanoparticles. We find that a large energy input (*i.e.*, heating α-MnAs nanoparticles to 330 °C in TOPO) is needed to drive the transformation from α-MnAs nanoparticles to β-MnAs nanoparticles, which are in turn kinetically trapped upon returning to room temperature. The large activation energy may suggest the presence of a low defect density in the nanoparticle cores,[26,27] which provides few sites for the first order structural phase transition to be nucleated (kinetic effect). Indeed, in MnAs nanodisks, considerable hysteresis was observed in the phase transition because nuclei need to form independently in each nanodisk, whereas in a bulk connected solid, generation and growth of a few nuclei are sufficient to induce the phase transformation over the materials' length scale.[28] Distinct from the prior work (which involved disks of significantly larger volume than the nanoparticles reported here), the structural pinning appears to be much larger in the discrete nanoparticles, hence the extreme temperature requirements for transformation. Alternatively to, or perhaps in concert with, kinetic trapping, the relative surface energies of the two structures (thermodynamic effects) may also play a role[26] as may the presence of the amorphous

shell; differentiating these factors is difficult in the absence of a body of data acquired as a function of crystallite size and amorphous shell thickness.

Magnetic Properties. The magnetization as a function of temperature for both the ca. 25 nm α- and β-MnAs nanoparticles were measured using zero-field-cooled (ZFC) and field-cooled (FC) measurement protocols. We also investigated the magnetic field dependence of the magnetization by measuring hysteresis loops. Based on the absence of structural transition from α to β noted in the temperature-dependent PXRD data (Figure 4), we predicted that the inherent ferromagnetism of α-MnAs samples would be maintained above 315 K (the first-order structural phase transition for bulk MnAs) up to ca. 400 K, the second order phase transition temperature, and the temperature believed to represent the true T_C of α-MnAs.[2] We also expected that these nanoscale particles would show superparamagnetism due to thermal spin fluctuation above the so-called blocking temperature (T_B). Superparamagnetism behavior has been noted in nanocomposites with MnAs nanoparticles of size 10−20 nm; but the large distribution in sizes that arise from bulk phase segregation methods led to a poorly defined T_B.[29] The large uniaxial magnetocrystalline anisotropy intrinsic to MnAs ensures that the larger particles (>50 nm) commonly prepared by epitaxial growth methods should be coercive up to T_C. The small size and narrow size distribution of the α-MnAs particles synthesized here should enable the superparamagnetic behavior to be more critically assessed. With respect to β-MnAs, the ability to study the low-temperature ($T < 315$ K) behavior of this phase should enable a detailed evaluation of the relationships between structure and magnetism at constant temperature, information that is not available in bulk phases due to the absence of a coexistence range for the α and β structures.

The results of magnetic measurements for α-MnAs are shown in Figures 5a and 5b, respectively, with the ZFC−FC magnetizations collected at **H** = 100 Oe. The α-MnAs sample shows a ferromagnetic transition (T_C) at 315 K, with the precise transition temperature determined using Arrott plots (inset to Figure 5a). Below this transition, the ZFC curve separates from the FC curve and shows a sharp peak at 310 K characteristic of the onset of superparamagnetic blocking. The α-MnAs magnetization develops hysteretic behavior with saturated magnetization at some temperature between 300 and 350 K (Figure 5b), also consistent with the onset of superparamagnetic blocking and the magnetic transition identified in the **M**(T) data. These data confirm that the 315 K transition is ferromagnetic, in agreement with measurements performed on bulk MnAs samples, and suggests that the magnetic phase is relatively pure.[1] The coercive field at 20 K is 550 Oe and decreases with increasing temperature, reaching zero by 350 K. The temperature dependent coercivity is indicative of the magnetic dynamics of the thermally blocked magnetic nanoparticles, rather than reflecting any intrinsic features of the ferromagnetism in these samples. The high blocking temperature (T_B = 310 K) noted for rather small (ca. 25 nm) particles can be attributed to the inherently large uniaxial magnetocrystalline anisotropy of MnAs, as previously described.[30] The room-temperature saturation magnetization of the α-MnAs nanoparticles is ~1×10^4 emu/mol of Mn (or 78 emu/g), which is 73% of the value reported for bulk MnAs (105.5 emu/g[31]). This yields an effective magnetic moment for α-MnAs nanoparticles of 1.8 μ_B/Mn as compared to 2.45 μ_B/Mn in bulk (using the standard factor of *ca.* 5500 to convert from emu/mol to μ_B/atom, assuming one magnetic Mn atom per mole of MnAs). Such reduction in the saturation magnetization is often observed in magnetic nanoparticles,[32] and can be attributed, at least in part, to the existence of nonmagnetic surface layers on the nanoparticles.

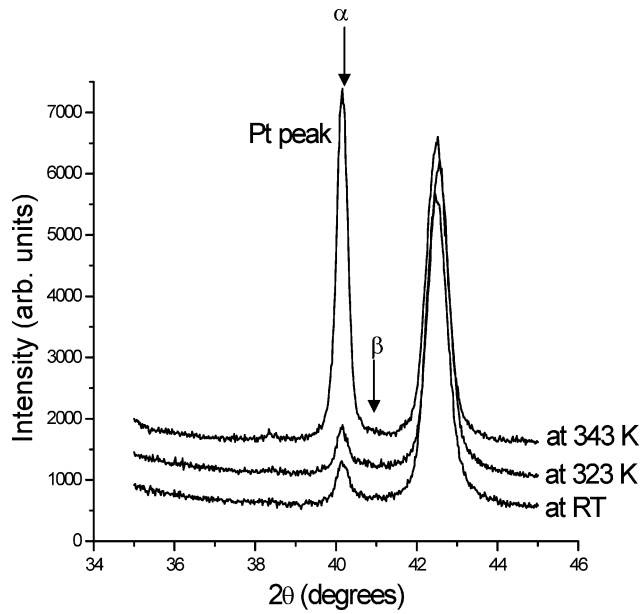

Figure 4. Temperature dependence of the PXRD patterns of α-MnAs nanoparticles heated *in situ* from room temperature to 343 K. "α" indicates the position of the characteristic peak for α -MnAs and "β" indicates the expected position of the β-MnAs peak. The Pt peak is due to the platinum heater upon which the sample is supported.

These magnetic measurements establish that α-MnAs nanoparticles are ferromagnetically ordered only up to ~315 K, despite the absence of any structural transformation in our discrete α-MnAs nanoparticles at this temperature (Figure 4). Additionally, the magnetization of the α-MnAs sample does not show any thermal hysteresis across the transition temperature, which would be expected if the magnetism were coupled to a structural change (Figure S2, Supporting Information). *These data suggest that the ferromagnetic transition is decoupled from any structural transition in α-MnAs nanoparticles.*

Rather surprisingly, the magnetic properties of β-MnAs nanoparticles are remarkably similar to those

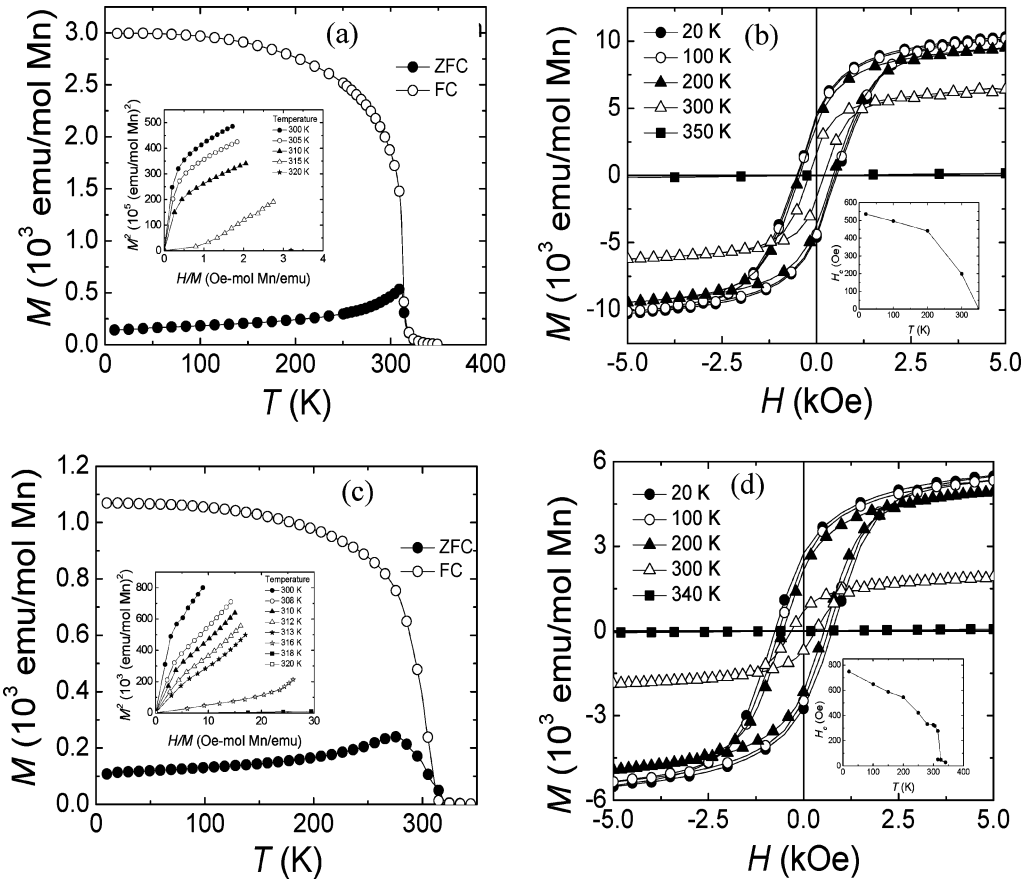

Figure 5. Graphs of magnetization (M) as a function of (a) temperature (*T*) measured at 100 Oe applied field using zero-field-cooled (ZFC) and field-cooled (FC) protocols and (b) applied field (H) for α-MnAs nanoparticles. (c and d) Corresponding data for β-MnAs nanoparticles. The insets show the generalized Arrot plots (a, c) and the coercive field as a function of the temperature (b, d) at which the hysteresis loop was measured.

of α-MnAs nanoparticles. The β-type sample also shows a magnetic transition near 315 K (again determined using an Arrott plot, shown in the inset to Figure 5c), attributed to a ferromagnetic transition; however, the separation between the ZFC and FC curves is more pronounced than seen for α-MnAs. Additionally, the ZFC curve of the β-type sample is much broader than that of the α-type sample, and there is a decrease in the blocking temperature (T_B = 275 K). This may be indicative of smaller nanoparticles (decreased T_B) as well as a broader range of particle sizes in the β-type sample (broader peak in ZFC), as suggested from the TEM histogram (Figure 3a), but could also point toward a slightly reduced magnetocrystalline anisotropy in β-MnAs as compared to α-MnAs. The β-MnAs sample exhibits coercive magnetic behavior at 300 K, which can be attributed to the presence of some fraction of unblocked nanoparticles at room temperature, and is consistent with the finite separation between the FC and ZFC curves at 300 K. The saturation moment of the β-type sample is 50% lower than that observed for α-MnAs (ca. 0.9 μ_B/Mn), while the coercive field at 20 K is larger (750 Oe) than for the α-MnAs sample (550 Oe).

Motivated by the similar magnetic properties exhibited by α-MnAs and β-MnAs nanoparticles and by literature reports suggesting the possibility of coexistence of both phases,[33] we have explored the possibility of observing time-dependent structural changes of β-MnAs nanoparticles. The powder diffraction patterns of β-MnAs nanoparticles held at room temperature indicate that the β-phase structure does transform to the thermodynamically stable α-phase over time (Figure 6a), but only very slowly (weeks-to-months). This is another manifestation of the phase-pinning noted previously when trying to transform α to β by heating, arising presumably due to the low defect densities in the individual nanoparticles and the necessity of nuclei being independently generated in each particle (note that even after 1 month, a significant part of the initial β-MnAs sample remains unchanged).

Within this framework, we investigated whether the similar magnetic properties of the α- and β-MnAs samples could arise from a small α-phase component in the β-phase samples, which gives rise to the anomalous ferromagnetic signal. This would also be consistent with the overall lower moment of β-MnAs relative to α-MnAs. If the magnetism in the β-phase samples is produced by a secondary α-phase contribution we would expect that the moment for the β-samples would increase over time, concomitant with the trans-

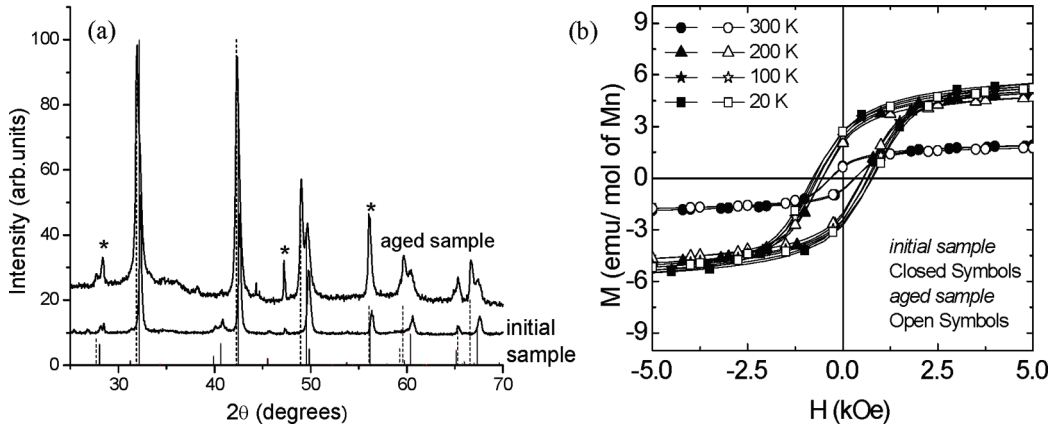

Figure 6. Comparison of PXRD patterns of β-MnAs nanoparticles (a) initial and aged for ca. 3 months along with (b) respective M *vs* H data. Vertical dotted lines correspond to the reference pattern of α-MnAs in panel (a) and vertical solid lines correspond to the reference pattern of β-MnAs. The stars denote the Si standard.

formation to α-phase. However, magnetic measurements of transformed samples show no change in the saturation magnetization ($\mathbf{M}_{sat}$) of the β-phase nanoparticles relative to the initially measured values (Figure 6b). Thus, we conclude that the observed ferromagnetism in the β-sample is intrinsic, and that ferromagnetic order with a Curie temperature of 315 K may be characteristic of MnAs in both crystal structures.

The appearance of ferromagnetic order in β-MnAs is unexpected, since undoped bulk orthorhombic MnAs is paramagnetic. On the other hand, the fact that bulk β-MnAs is only stable above 315 K means that the low-temperature magnetic behavior in the orthorhombic structure is essentially unknown. Some indication of the intrinsic behavior of β-MnAs below 315 K can be gleaned by comparison to phosphorus-doped MnAs, which adopts exclusively the β (MnP) structure for doping levels of >4%. In addition to stabilizing the orthorhombic MnP structure, P doping in MnAs above a critical concentration of approximately 15% can produce a ferromagnetically ordered state, having a Curie temperature of approximately 245 K for $MnAs_{0.82}P_{0.18}$.[34] This shows that the β structure is not inimical to the development of ferromagnetism in MnAs. It has been suggested that Mn undergoes a change from a high spin state in the NiAs structure to a low spin state in the MnP structure.[2] This is consistent with studies on the magnetization of MnAs, which show that reducing the volume leads to a reduction in the net moment.[35] Accordingly, the smaller volume of β-MnAs (33.33 Å^3/formula unit) relative to α-MnAs (34.10 Å^3/formula unit) nanoparticles could be a contributing factor for the reduction in the saturation magnetization in the β structure as compared to the α structure. However, this suggestion would need to be investigated through direct measurements of the Mn moment in both samples, and may not agree with the magnetization curves for partially converted samples (Figure 6b), which show very similar moments regardless of the α to β phase ratio.

An alternative explanation for the reduction of the β-MnAs moment relative to the α-MnAs moment, despite very similar magnetic transition temperatures, may be found in a more detailed study of the nanoparticle structures. The magnetic moment of each sample was calculated on the basis of the Mn content in the sample, assuming that MnAs is the only contributor. However, if Mn is also present in some additional secondary phase, with different impurity fractions for the α- and β-forms, this could account for the differences in saturation magnetization between the two structures. While we see no evidence of a separate secondary phase by PXRD or TEM, we do see an amorphous shell in both types of MnAs nanoparticles. The differences in magnetic moment could be explained if this shell contains nonferromagnetic Mn, and if it is present in differing amounts in the two samples. We have calculated the shell and core volumes and shell/core (S/C) ratios for both types of MnAs particles using TEM analysis (Table 1). We find that the S/C ratio of β-MnAs is significantly greater than that of α-MnAs (0.85 *vs* 0.65), which would be consistent with the smaller magnetization observed in β-MnAs, given that the core (ferromagnetic) volumes of both phases are of similar size.

To characterize the chemical characteristics of the amorphous shell, we performed infrared spectroscopy on the samples. Similar patterns were obtained for the α- and β-samples, and a representative pattern is shown in Figure 7. Peaks appearing at 782 and 483 cm^{-1} can be attributed to either As−O or Mn−O stretches,[36,37] whereas the band at 653 cm^{-1} and two smaller bands at 1040 and 1130 cm^{-1} can be attributed to As−O stretching.[37] Therefore, we propose that the amorphous shell of MnAs nanoparticles may comprise nonferromagnetic species such as $MnAsO_z$,[38,39] Mn_aO_b,[40] and/or As_xO_y. This would reduce the effective moment per Mn arising from the crystalline MnAs nanoparticle core, leading to a smaller magnetization for β (which has a thicker shell) than the α-MnAs nanoparticles.

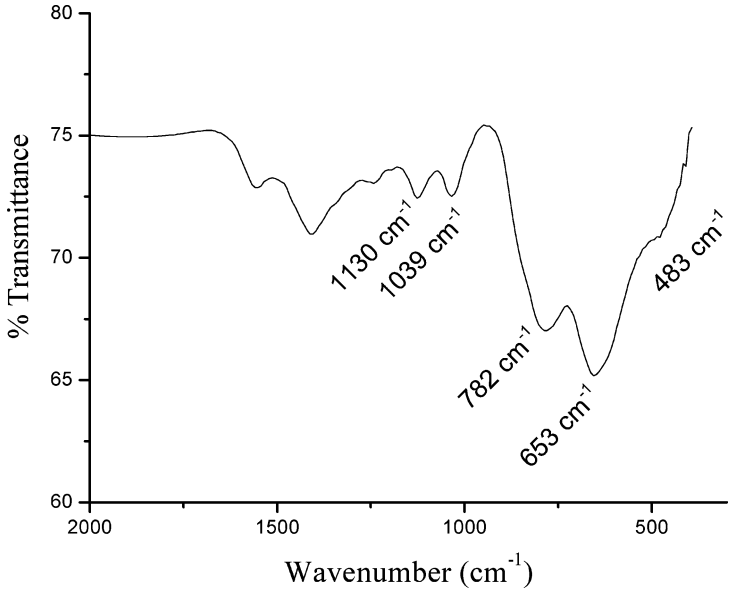

Figure 7. IR spectrum of a sample of β-MnAs nanoparticles showing the Mn−O and As−O stretching vibrational bands. Similar spectra were obtained for α-MnAs nanoparticles.

A separate possibility that could explain both the reduced moment and the similarity in properties is that the ferromagnetism arises, at least in part, from the amorphous magnetic shell, which makes up different percentages of the sample in each case. Based on the close similarity between the observed magnetic behavior of our nanoparticles and that of bulk crystalline MnAs, it seems unlikely that this would arise from an amorphous oxide phase. However, we cannot rule out the possibility of an amorphous MnAs phase present in both samples, which could be contributing to the magnetism.

CONCLUSIONS

We have successfully prepared thermodynamically stable α-MnAs and metastable β-MnAs nanoparticles in the absence of a support by developing a solution-phase arrested precipitation method. Rapid nucleation at high temperature (330 °C) favors formation of β-MnAs, whereas α-MnAs is only formed upon slow nucleation at much lower temperatures (250 °C). As discrete nanoparticles, both phases are kinetically trapped, so that conversion of β to α (the thermodynamic phase at room temperature) requires periods of weeks-to-months to achieve at room temperature. Likewise, the first order structural phase transition from α to β MnAs at 315 K (characteristic of bulk MnAs) is not observed over the time scale of temperature-dependent PXRD studies (hours). These data suggest structural pinning in the nanoparticles, perhaps attributed to a low defect density. Epitaxially prepared nanoparticles and disks often show phase coexistence and hysteresis near the phase transition temperature, but there have been no reports of the kinds of enhanced kinetic stabilities (weeks to months) that we have encountered in the solution-phase prepared samples. Intriguingly, despite the absence of a structural phase transition, the ferromagnetic phase transition that occurs concomitantly with the structure transition in bulk MnAs, is still observed at 315 K, and is found in both α and β phases. This suggests that the magnetic transition is insensitive to substantial changes in structure, a surprising result. Current studies are focused on pair distribution function (PDF) analysis of temperature-dependent synchrotron data and Raman studies, which will enable us to correlate small structural perturbations to the observed magnetic transition and identify amorphous MnAs, if present.

METHODS

Materials and Methods. All preparations of precursor mixtures were performed inside of an argon-filled glovebox and reactions were carried out under inert atmosphere conditions on a Schlenk line. Isolation of the nanoparticles was performed under ambient conditions. Dimanganese(0) decacarbonyl (Mn_2CO_{10}, Aldrich, 98%), triphenylarsine oxide (Ph_3AsO, Aldrich, 97%), 1-octadecene (Aldrich, 90%), chloroform (Fisher, 99.9%), and absolute ethanol (AAPER), were used as purchased. Trioctylphosphine oxide (TOPO, Aldrich, 90%) was distilled prior to use.

Preparation of α- and β-MnAs Nanoparticles. For the preparation of β-MnAs, Mn_2CO_{10} (0.256 mmol) was mixed with Ph_3AsO (0.528 mmol) and 8.0 mL of 1-octadecene in a Schlenk flask inside an argon-filled glovebox and then removed to the Schlenk line. The mixture was heated slightly with a heat gun to dissolve the solid precursors prior to injection. This yellow colored mixture was cannulated under inert conditions into hot TOPO (5.0 g) and heated at 330 °C for 18 h. Before the isolation of nanoparticles, the reaction temperature was reduced to 50 °C. Nanoparticles were isolated by dispersing in chloroform and precipitating with absolute ethanol under ambient atmosphere. The black precipitate of nanoparticles was isolated by centrifugation. An alternative slow heating method, which slowly heats all the precursors and coordinating agents in one flask up to 330 °C, with continued heating at 330 °C for 18 h, also produces β-MnAs nanoparticles. If desired, isolated nanoparticles could be redissolved and reprecipitated several times with chloroform and ethanol, respectively, to wash off coordinating TOPO groups from the surface.

The preparation of α-MnAs nanoparticles was carried out by following a similar method to the β-MnAs synthesis utilizing a slow heating method to 250 °C. A flask containing all the reaction components was heated slowly up to 200 °C over a ca. 2 h period and then the temperature was ramped up to 250 °C in one step. The reaction was left at 250 °C for 18 h. The isolation of nanoparticles is the same as described for β-MnAs nanoparticles.

Powder X-ray Diffraction (PXRD). A Rigaku RU 200B X-ray diffractometer with a Cu Kα rotating anode source was used for X-ray powder diffraction analysis. The powdered MnAs nanoparticles were ground with a small amount of vacuum grease and silicon standard and placed on a zero background quartz (0001) holder. The X-ray pattern was identified by comparison to phases in the Powder Diffraction File (PDF) database (ICDD, release 2000).

Transmission Electron Microscopy (TEM). A JEOL FasTEM 2010 HR TEM operating at 200 kV was employed for sample imaging. Samples were dispersed in chloroform and a drop of the resultant colloid was placed on a carbon-coated copper grid and allowed to dry at room temperature under ambient conditions. The images were collected in bright field mode. The histograms were com-

puted on the basis of the core particle sizes obtained using Scion Image Software. The average particle size for elliptical α-MnAs particles was calculated by measuring the diameter along the small axis. Approximately 320 and 450 particles of α-type and β-type samples, respectively, were measured to compute the histograms.

Energy Dispersive Spectroscopy (EDS). A Hitachi S-2400 scanning electron microscope equipped with an EDAX inc. detector was used to collect EDS data on the nanoparticles. A small amount of dry sample was put on carbon tape adhered to an aluminum sample holder. The Genesis Software was used to collect the EDS data and subsequently to analyze semiquantitative elemental compositions using Kα lines of Mn, As, and P.

Infrared Spectroscopy. A Varian FTS 3000 MX FTIR spectrometer was used to investigate chemical features of the nanoparticles. Powdered samples of MnAs nanoparticles were mixed with KBr (~1:10 ratio) and ground to yield a uniform mixture. The mixture was pressed into a transparent pellet by applying 2000 psi pressure using a Carver hydraulic pellet press and 13 mm die set; FTIR data were acquired on the resultant KBr pellet.

SQUID Magnetometry. The dc magnetic susceptibility was measured using a Quantum Design MPMS-5S SQUID magnetometer. To make magnetic measurements, the sample was processed into a fine powder and vacuum sealed inside a quartz tube. The tube was then mounted in a straw for attachment to the sample probe. The temperature dependent dc magnetization was measured using a zero-field-cooled (ZFC) protocol from 10 to 350 K in a measuring field of 100 Oe. The measurement was then repeated over the same temperature range and measuring field using a field-cooled (FC) protocol in a cooling field of 100 Oe. The field dependent dc magnetic susceptibility was measured over a range of −5 to +5 kOe at temperatures ranging from 20 up to 350 K.

Acknowledgment. We acknowledge the National Science Foundation (DMR-0701161), the donors of the American Chemical Society (PRF No. 46160-G10), and the Wayne State University Institute of Manufacturing Research for financial support provided for this research. Electron microscopy was conducted in the Laboratory for Analytical Electron Microscopy at WSU on a JEOL 2010 F purchased under NSF Grant DMR-0216084. We also thank C. Lind, S. Gates, and P. Burckel from the University of Toledo for assisting in collection of temperature dependent PXRD data and J. Musfeldt from the University of Tennessee, Knoxville, for preliminary infrared spectroscopy data.

Supporting Information Available: Chemical analysis and temperature-dependent magnetic susceptibility data taken upon heating and cooling through the magnetic transition. This material is available free of charge *via* the Internet at http://pubs.acs.org.

REFERENCES AND NOTES

1. Ishikawa, F.; Koyama, K.; Watanabe, K.; Wada, H. Field Induced Structural Transformation in MnAs. *Jpn. J. Appl. Phys.* **2003**, *42*, 918–920.
2. Goodenough, J. B.; Kafalas, J. A. High-Pressure Study of the First-Order Phase Transition in MnAs. *Phys. Rev.* **1967**, *157*, 389–395.
3. Iikawa, F.; Brasil, J. J. S. P.; Adriano, C.; Couto, O. D. D.; Giles, C.; Santos, P. V.; Däweritz, L.; Rungger, I.; Sanvito, S. Lattice Distortion Effects on the Magnetostructural Phase Transition of MnAs. *Phys. Rev. Lett.* **2005**, *95*, 077203−1-4.
4. Suzuki, T.; Ido, H. Relation between Structural and Magnetic Properties of Compound $MnAs_{1-x}P_x$ ($0 \leq x \geq 0.275$). *J. Phys. Soc. Jpn.* **1982**, *51*, 3149–3156.
5. Mira, J.; Rivadulla, F.; Rivas, J.; Fondado, A.; Guidi, T.; Caciuffo, R.; Carsughi, F.; Radaelli, G. G.; Goodenough, J. B. Structural Transformation Induced by Magnetic Field and "Colossal-Like" Magnetoresistance Response above 313 K in MnAs. *Phys. Rev. Lett.* **2003**, *90*, 097203−1-4.
6. Gama, S.; Coelho, A. A.; Campos, A. A.; Carvalho, M.; Gandra, F.; Von Ranke, P. J.; De Oliveira, N. A. Pressure-Induced Colossal Magnetocaloric Effect in MnAs. *Phys. Rev. Lett.* **2004**, *93*, 237202−1-4.
7. Von Ranke, P. J.; Gama, S.; Coelho, A. A.; Campos, A.; Carvalho, M.; Gandra, F.; De Olivera, N. A. Theoretical Description of the Colossal Entropic Magnetocaloric Effect: Application to MnAs. *Phys. Rev. B* **2006**, *73*, 014415−1-5.
8. Takagaki, Y.; Herrmann, C.; Wiebicke, E.; Herfort, J.; Daweritz, L.; Ploog, K. H. Slow Relaxation of Manetization in MnAs Nanomagnets on GaAs(001). *Appl. Phys. Lett.* **2006**, *88*, 032504.
9. Hai, P. N.; Sakata, Y.; Yokoyama, M.; Ohya, S.; Tanaka, M. Spin-Valve Effect by Ballistic Transport in Ferromagnetic Metal (MnAs)/Semiconductor (GaAs) Hybrid Heterostructures. *Phys. Rev. B* **2008**, *77*, 214435−1-6.
10. Ramlan, D. G.; May, S. J.; Zheng, J. G.; Allen, J. E.; Wessels, B. W.; Lauhon, L. J. Ferromagnetic Self-Assembled Quantum Dots on Semiconductor Nanowires. *Nano. Lett.* **2006**, *6*, 50–54.
11. Kaganer, V. M.; Jenichen, B.; Schippan, F.; Braun, W.; Däweritz, L.; Ploog, K. H. Strain-Mediated Phase Coexistance in Heteroepitaxial Films. *Phys. Rev. Lett.* **2000**, *85*, 341–344.
12. Takagaki, Y.; Jenichen, B.; Herrmann, C.; Weibicke, E.; Däweritz, L.; Ploog, K. H. First-Order Phase Transition in MnAs Disks on GaAs (001). *Phys. Rev. B* **2006**, *73*, 125324−1-5.
13. Park, J.; Joo, J.; Kwon, S. G.; Jang, Y.; Hyeon, T. Synthesis of Monodisperse Spherical Nanocrystals. *Angew. Chem., Int. Ed.* **2007**, *46*, 4630–4660.
14. Vasquez, Y.; Henkes, A. E.; Bauer, J. C.; Schaak, R. E. Nanocrystal Conversion Chemistry: A Unified and Materials-General Strategy for the Template-based Synthesis of Nanocrystalline Solids. *J. Solid State Chem.* **2008**, *181*, 1509–1523.
15. Brock, S. L.; Perera, S. C.; Stamm, K. L. Chemical Routes for Production of Transition-Metal Phosphides on the Nanoscale: Implications for Advanced Magnetic and Catalytic Materials. *Chem.—Eur. J.* **2004**, *10*, 3364–3371.
16. Brock, S. L.; Senevirathne, K. Recent Developments in Synthetic Approaches to Transition Metal Phosphide Nanoparticles for Magnetic and Catalytic Applications. *J. Solid State Chem.* **2008**, *181*, 1552–1559.
17. Battaglia, D.; Peng, X. Formation of High Quality InP and InAs Nanocrystals in a Noncoordinating Solvent. *Nano Lett.* **2002**, *2*, 1027–1030.
18. Fanfair, D. D.; Korgel, B. A. Bismuth Nanocrystal-Seeded III−V Semiconductor Nanowire Synthesis. *Cryst. Growth Des.* **2005**, *5*, 1971–1976.
19. Green, M. Solution Routes to III−V Semiconductor Quantum Dots. *Curr. Opin. Solid State Mater. Sci.* **2002**, *6*, 355–363.
20. Lu, J.; Xie, Y.; Jiang, X.; He, W.; Du, G. A Safe Sonochemical Route to Iron, Cobalt and Nickel Monoarsenides. *J. Mater. Chem.* **2001**, *11*, 3281–3284.
21. Wei, S.; Lu, J.; Yu, W.; Zhang, H.; Qian, Y. $Ni_{11}As_8$ Single-Crystalline Nanosheets *via* Hydrothermal Redox Route. *Inorg. Chem.* **2005**, *44*, 3844–3849.
22. Barry, B. M.; Gillan, E. G. Low-Temperature Solvothermal Synthesis of Phosphorus-Rich Transition-Metal Phosphides. *Chem. Mater.* **2008**, *20*, 2618–2620.
23. Iikawa, F.; Brasil, M. J. S. P.; Adriano, C.; Couto, O. D. D.; Giles, C.; Santos, P. V.; Däweritz, L.; Rungger, I.; Sanvito, S. Lattice Distortion Effects on the Magnetostructural Phase Transition of MnAs. *Phys. Rev. Lett.* **2005**, *95*, 077203−1-4.
24. Zieba, A.; Shelte, K.; Kjeshus, A.; Andersen, A. F. Phase Transitions in MnAs. *Acta Chem. Scand.* **1978**, *A32*, 173–177.
25. Bose, C.; Thangadurai, P.; Ramasamy, S.; Ganesan, V.; Asokan, S. Nonlinear *I*−*V* Characteristics of Nanocrystalline SnO_2. *Nanotechnology* **2006**, *17*, 1752–1757.
26. Chen, C.; Herhold, A. B.; Johnson, C. S.; Alivisatos, A. P. Size Dependence of Structural Metastability in Semiconductor Nanocrystals. *Science* **1997**, *276*, 398–401.
27. Jacobs, K.; Wickham, J.; Alivisatos, A. P. Threshold Size for Ambient Metastability of Rock-Salt CdSe Nanocrystals. *J. Phys. Chem. B* **2002**, *106*, 3759–3762.

28. Jenichen, B.; Takagaki, Y.; Ploog, K. H.; Darowski, N.; Feyerherm, R.; Zizak, I. Nucleation at the Phase Transition Near 40 C in MnAs Nanodisks. *Appl. Phys. Lett.* **2006**, *89*, 051915−1-3.
29. Kwiatkowski, A.; Wasik, D.; Kamińska, M.; Bożek, R.; Szczythko, J.; Twardowski, A.; Borysiuk, J.; Sadowski, J.; Gosk, J. Structure and Magnetism of MnAs Nanocrystals Embedded in GaAs as a Function of Post-Growth Annealing Temperature. *J. Appl. Phys.* **2007**, *101*, 113912−1-6.
30. Takagaki, Y.; Herrmann, C.; Wiebicke, E.; Herfort, J.; Däweritz, L.; Ploog, K. H. Slow Relaxation of Magnetization in MnAs Nanomagnets on GaAs (001). *Appl. Phys. Lett.* **2006**, *88*, 032504−1-3.
31. Das, A. K.; Pampuch, C.; Ney, A.; Hesjedal, T.; Däweritz, L.; Koch, R.; Ploog, K. H. Ferromagnetism of MnAs Studied by Heteroepitaxial Films on GaAs(001). *Phys. Rev. Lett.* **2003**, *91*, 087203−1-4.
32. Serna, C. J.; Bodker, F.; Morup, S.; Morales, M. P.; Sandiumenge, F.; Veintemillas-Verdaguer, S. Spin Frustration in Maghemite Nanoparticles. *Solid State Commun.* **2001**, *118*, 437–440.
33. Kaganer, V. M.; Jenichen, B.; Schippan, F.; Braun, W.; Däweritz, L.; Ploog, K. H. Strain-Mediated Phase Coexistance in MnAs Heteroepitaxial Films on GaAs: An X-ray Diffraction Study. *Phys. Rev. B* **2002**, *66*, 045305−1-9.
34. Fjellvåg, H.; Andresen, A. F.; Bärner, K. On the Magnetic and Structural Properties of the $MnAs_{1-x}P_x$ System ($x \leq 0.18$). *J. Magn. Magn. Mater.* **1984**, *46*, 29–39.
35. Maki, K.; Kaneko, T.; Hiroyoshi, H.; Kamigaki, K. Crystalline and Magnetic Properties of MnAs Under Pressure. *J. Magn. Magn. Mater.* **1998**, *177−181*, 1361–1362.
36. Chertihin, G. V.; Andrews, L. Reactions of Laser-Ablated Manganese Atoms with Dioxygen. Infrared Spectra of MnO, OMnO, $Mn(O_2)$, $(MnO)_2$, and Higher Oxide Complexes in Solid Argon. *J. Phys. Chem. A* **1997**, *101*, 8547–8553.
37. Szymanski, H. A.; Marabella, L.; Hoke, J. J. H. Infrared and Raman Studies of Arsenic Compounds. *Appl. Spectrosc.* **1968**, *22*, 297–304.
38. Aranda, M. A. G.; Attfield, J. P.; Batchelor, E.; Shields, G.; Bruque, S.; Gabas, M. Simultaneous Antiferromagnetic Order and Spin-Glass-like Behavior in $MnAsO_4$. *Inorg. Chem.* **1998**, *37*, 1329–1335.
39. Aranda, M. A. G.; Bruque, S.; Attfield, J. P.; Palacio, F.; Von Dreele, R. B. Changes in Magnetic Couplings after Chimie Douce Reactions: Magnetic Structures of $LiMnXO_4(OD)$ (X = P, As). *J. Solid. State Chem.* **1997**, *132*, 202–212.
40. Rudolf, T.; Kant, C.; Mayr, F.; Loidl, A. Magnetic-Order Induced Phonon Splitting in MnO from Far-Infrared Spectroscopy. *Phys. Rev. B* **2008**, *77*, 024421−1-5.